Fatigue Assessment of Crane Rail Welds by Local Concepts

M. Euler[1] and U. Kuhlmann[1]

[1] University of Stuttgart, Institute of Structural Design, Pfaffenwaldring 7, 70569 Stuttgart, Germany, mathias.euler@ke.uni-stuttgart.de, u.kuhlmann@ke.uni-stuttgart.de

ABSTRACT. The introduction of the wheel loads into a crane runway with a hot rolled I-section and a block rail fastened by longitudinal fillet welds forms a multiaxial fatigue problem. At the point of wheel load application the upper part of the runway girder is subjected to a stress field comprising local stress components induced by the concentrated load, i. e. local transverse pressure $\sigma_{z,local}$ and local shear stress $\tau_{xz,local}$, in addition to the global stress components σ_x und τ_{xz} due to global bending. The superposition of all aforementioned stress components (and stress ranges, resp.) during each single crane pass results in a non-proportional cyclic stressing of the rail welds. This paper compares the results of different local concepts for the fatigue evaluation of the wheel load application with measurements of girder tests.

INTRODUCTION

At the point of wheel load application the upper part of the runway girder (Figs 1a, 1b) is generally subjected to a stress field comprising local stress components induced by the concentrated load, i. e. local transverse pressure $\sigma_{z,local}$ and local shear stress $\tau_{xz,local}$, in addition to the global stress components σ_x und τ_{xz} due to global bending. Fig. 1c illustrates the stress history at midspan location of a single-span crane runway girder caused by a travelling crane assuming constant travelling velocity. Since the crane possesses two crane wheels each passage of the crane causes two wheel passages. The amplitudes of σ_x and $\sigma_{z,local}$ appear at the same time despite that the frequency of $\sigma_{z,local}$ is twice as large as that of σ_x. The fact that the stresses $\sigma_{z,local}$ and $\tau_{xz,local}$ have to be inherently out of phase is illustrated in Fig. 1d. Subsequently, the stressing of the considered crane runway system indicates a permanent shift of the principal stress directions and has to be referred to as non-proportional.

Basically, the computed nominal stresses of a crane runway differ from the real stressing for three reasons: (i) The welding of the crane rail leads to material homogeneities, and residual stresses are induced by the welding procedure. (ii) The shape of the weld toes and roots forms a geometric notch amplifying the nominal stresses. (iii) The concentrated load causes local stress peaks as described above. Altogether, the crane runway undergoes a multiaxial stressing turning the wheel load application into a complex fatigue problem with non-proportional loading and several stress-rising effects.

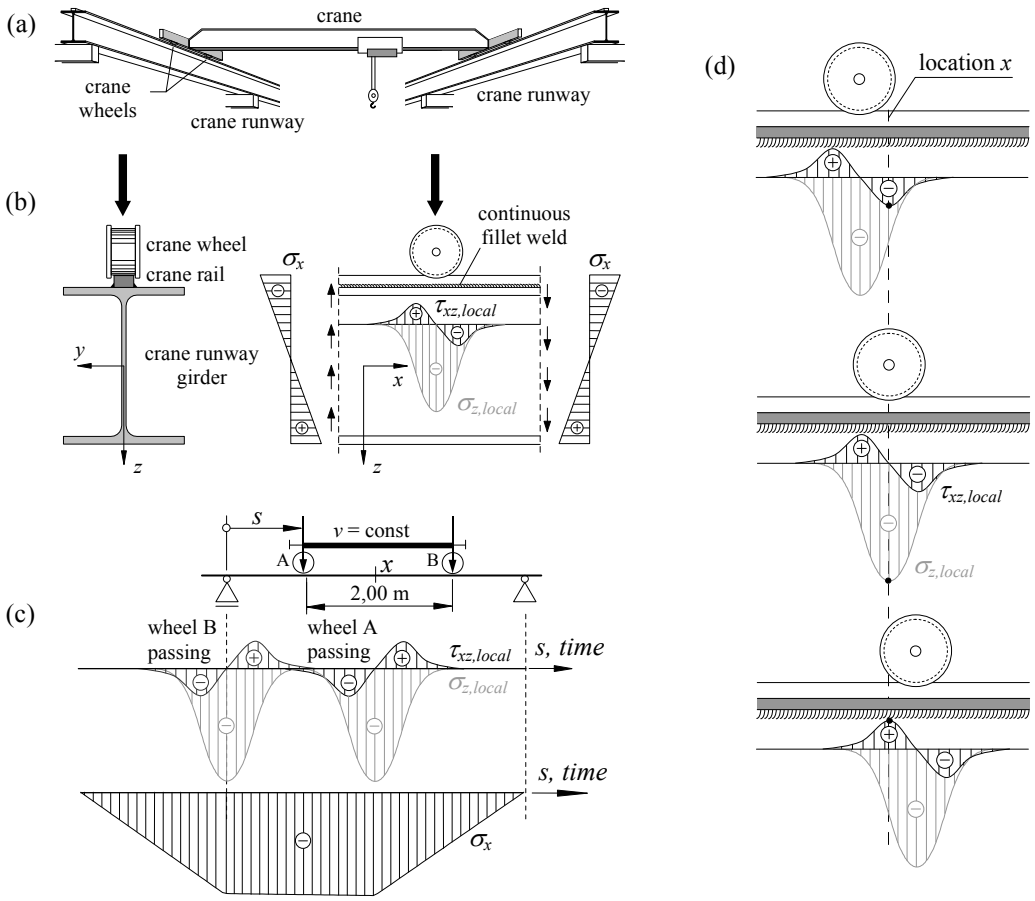

Figure 1. Overhead travelling crane on crane runways (a), typical cross section of a crane runway for light and moderate crane service (b), stress history caused by one crane passage at midspan location x = 2,00 m in case of a single-span runway (L = 4,00 m) (c), three states of stress for particular wheel locations (d). Remark: Global shear stress τ_{xz} is not considered for the sake of simplicity

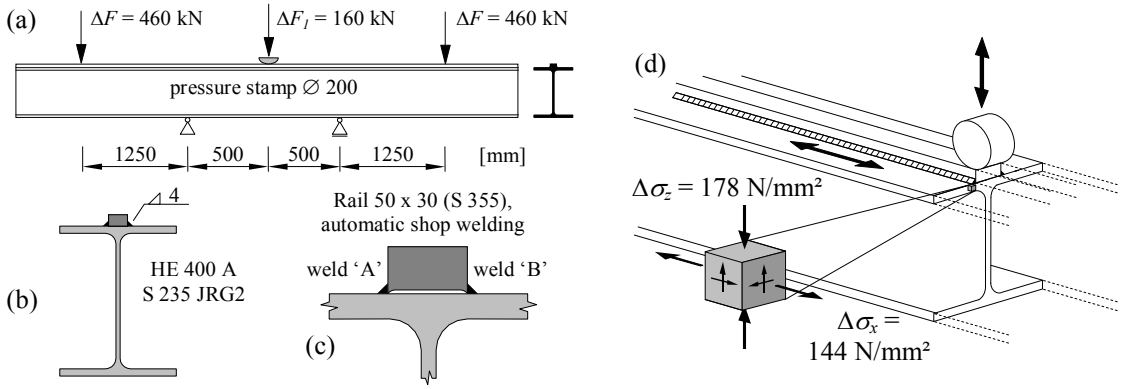

Figure 2. Test set-up (a), cross section (b), interface between crane rail and upper flange (c), state of stress in terms of nominal stresses (d)

EXPERIMENTAL INVESTIGATION

In a research project of the Deutsche Ausschuss für Stahlbau (DASt) under funding of AiF as part of the IGF-program of the German Federal Ministry of Economics and Technology (BMWi) the fatigue strengths of crane runway girders with particular focus on the load application were determined. Only the two test girders #2 and #3 with continuous rail welds are going to be considered in this paper. All loads acted in phase with constant amplitudes, $R \approx 0.1$. For more details see Figs 2a, 2b and [4].

In the tests the bottom rail surface (Fig. 2c) was recessed to avoid any contact between rail and girder and to ensure that the load transfer from the rail to the top flange was exclusively realized by the rail welds. Hence, all loads acting on the top surface of the rail were transmitted into the top flange by the rail welds. With the test set-up only an interaction of longitudinal stress σ_x and transverse pressure σ_z could be achieved at the point of wheel load application, Fig. 2d. It did not allow the superposition of these stress components together with the local shear stress $\tau_{xz,local}$, compare Fig. 1d.

The observed failure mode comprised three phases, Figs 3a - 3d. The so-called primary crack was initiated at the bottom surface of the rail right below the wheel load (phase 1). After the rail through-crack the rail welds failed in a ductile manner (phase 2). Subsequently, the crack propagated into the top flange leading to two crack growth centres (phase 3). Presumably, during phase 2, secondary cracks to each side of the rail developed right beneath the wheel load along the weld toes, see Fig. 3b. These cracks were hardly detectable. Their fracture plane was oriented normal to that of the primary crack. The number of load cycles at crack initiation in the rail was about 700,000 for test girder #2 and about 640,000 for test girder #3. Note that in [4] and [5] the load cycles to failure are 762,000 and 700,000 since there the failure criterion was rail through-cracking instead of crack initiation.

NUMERICAL INVESTIGATION

The fully elastic notch stresses were computed by a Finite-Element Analysis (FEA) using the software package ANSYS Version 11. Basically, the stress determination was subdivided into two steps. Firstly, a global model with a coarse mesh was set up comprising the tested crane runway girder between the supports together with the crane wheel (contact problem) taking advantage of the symmetry. Secondly, a 3-D submodel was created in order to refine the results of the global model. The weld toes and the weld roots were rounded off with a fictitious radius $\rho_f = 1$ mm [12]. The strain measurements at the flange to web junction at the loading section recorded during the cyclic testing served for the validation of the generated model. The FE strains of the global model and the measured strains have shown a very good fit. See [1] for details.

The assessment of the local stresses was primarily carried out along paths at the weld notches. The maximum stress components per path were determined for the assessment, Tab. 1. Because of a smaller weld toe angle weld ‘A’ exhibits higher stresses. In the following the focus is laid on the assessment of the secondary crack, Figs 3e - 3k.

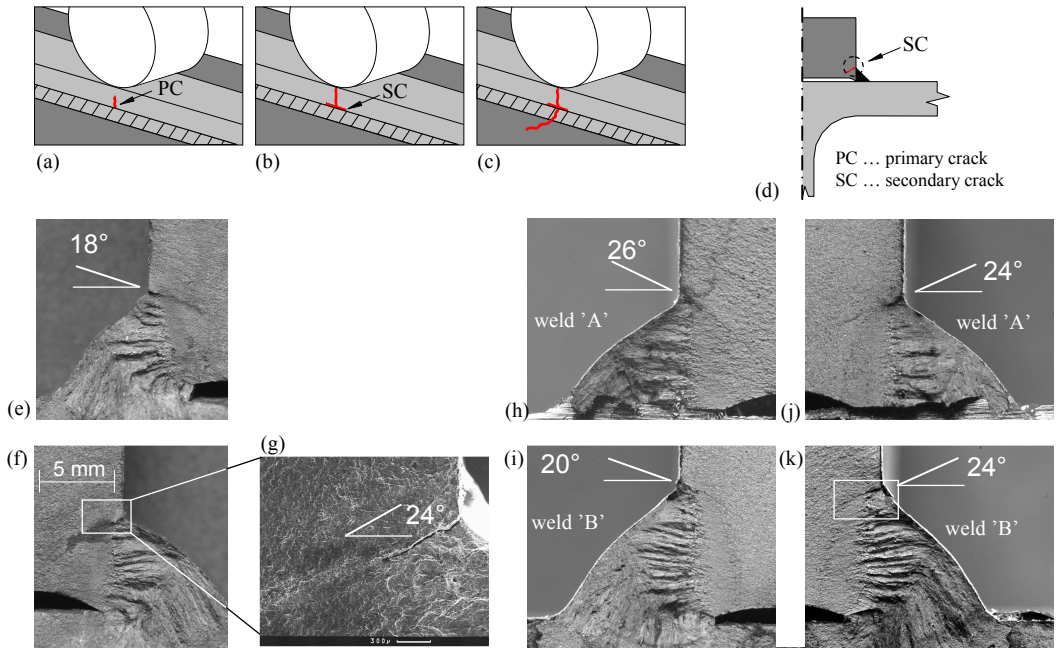

Figure 3. General failure mode (a)-(d), crack surfaces together with the early secondary crack growth orientation of girder #2 (e)-(g), and of weld 'A' (h)-(i) and 'B' (j)-(k) of girder #3

Table 1. Notch stresses at the upper weld toe of weld 'A' (values of weld 'B' in parentheses) at planes of different angle θ (N/mm²)

θ [°]	-90	0	15	**20**	25	**30**	35	90
$\sigma_{n,max}$	0	0	0	0	0	0	0	0
$\sigma_{n,min}$	-226	-712	-527	-459	-392	-326	-266	-226
$\Delta\tau_n$	305	305	386	390	382	363	333	305
$\Delta\tau_{eff}$	305	305	386	**390** (337)	382	363	333	305
$\Delta\sigma_{eq}$				**675** (583)				
$\Delta\tau_{eff,mod}$	237	91	228	252	264	**265** (237)	253	237
$\Delta\sigma_{eq,mod}$						**459** (410)		

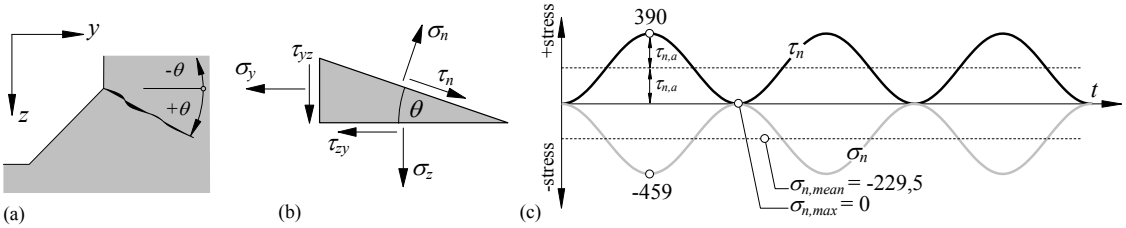

Figure 4. Orientation of critical planes at upper weld toe (a), stresses at any plane with angle θ (b), stress history of the components σ_n and τ_n of the plane with $\theta = 20°$ (c)

FATIGUE ASSESSMENT

Findley's hypothesis

Due to the outcome of the girder tests only planes at the upper weld toe have to be considered making an angle θ with the *y*-axis, Fig. 4a. It holds for the stresses at such planes (Fig. 4b):

$$\sigma_n = \sigma_y \cdot \sin^2\theta + \sigma_z \cdot \cos^2\theta + 2 \cdot \tau_{yz} \cdot \sin\theta \cdot \cos\theta \tag{1}$$

$$\tau_n = \left(\sigma_y - \sigma_z\right) \cdot \sin\theta \cdot \cos\theta + \tau_{yz} \cdot \left(\cos^2\theta - \sin^2\theta\right) \tag{2}$$

$$\frac{\Delta\tau_{eff}}{2} = \tau_{eff,a} = \tau_{n,a} + k \cdot \sigma_{n,\max} \tag{3}$$

The effective shear stress range $\Delta\tau_{eff}$ according to Findley [2] only depends on the maximum (positive) normal stress $\sigma_{n,max}$ and the maximum alternating shear stress $\tau_{n,a}$ at the considered plane. From the stress history in Fig. 4c it can be seen that the greatest positive normal stress becomes $\sigma_{n,max} = 0$ in all planes. Subsequently, the normal stress has no influence on the effective shear stress range $\Delta\tau_{eff}$, Tab. 2. Additionally, a modified $\Delta\tau_{eff,mod}$ is determined that is received if using the mean stress $\sigma_{n,mean}$ instead of the maximum positive normal stress $\sigma_{n,max}$. The orientation of the critical plane in the first case amounts to 20° and in the second case to 30°, Tab. 2. That is in good agreement with the measurements, Figs 3e - 3k. For further considerations the effective shear stress ranges are transformed in equivalent normal stress ranges according to distortion energy hypothesis (DEH) by applying $\Delta\sigma_{eq}^2 = \Delta\tau_{eq}^2 \cdot \sqrt{3}$.

Effective equivalent stress hypothesis (EESH)

The loading of the test girders did not exhibit any phase shift ($\delta = 0$), consequently, the computation of the effective equivalent stress according to EESH [11] simplifies solely to Eq. 5 since the second and third term of Eq. 4 become unity.

$$\Delta\sigma_{eq}(\delta) = \Delta\sigma_{eq}(\delta = 0°) \cdot \frac{F(\delta)}{F(\delta = 0°)} \cdot \sqrt{G^{1-\left(\frac{\delta - 90°}{90°}\right)^2}} \tag{4}$$

$$\Delta\sigma_{eq}(\delta = 0°) = \sqrt{\Delta\sigma_x^2 + \Delta\sigma_y^2 - \Delta\sigma_x \cdot \Delta\sigma_y + f_s \cdot 3 \cdot \Delta\tau_{xy}^2} \tag{5}$$

$$f_s = \frac{\Delta\sigma_{eq,axial}}{\Delta\sigma_{eq,shear}} \tag{6}$$

Therefore, the effective equivalent stress depends only on the stress ranges and the factor f_s that captures the so-called micro-support size effect and can be expressed by Eq. 6 with $\Delta\sigma_{eq,axial}$ and $\Delta\sigma_{eq,shear}$ as the supportable effective equivalent stress with a survival probability of 50 % under pure bending/axial loading and pure shear according to DEH.

The exact computation of the size effect factor f_s requires statistically proven *S-N* curves for the considered constructional detail under pure bending/axial loading and pure shear. Since such specific information is not available for the welded crane rail this factor has to be estimated. In [8] fillet welds under pure shear stress $\Delta\tau_{nom}$ due to torsion were tested, Tab. 3. The determined supportable shear stress ranges represent primarily weld root failure. Thus, these values are conservative concerning the fatigue strength of the weld toe. The supportable notch stress ranges $\Delta\tau_{notch}$ and the corresponding equivalent stress ranges $\Delta\sigma_{eq,shear}$ according to DEH can be computed as given by Eq. 7. The stress concentration is estimated based on the notch stress concentration factor α_τ of *Neuber* [7] for a shallow notch, Fig. 5.

$$\Delta\sigma_{eq,shear} = \Delta\tau_{notch} \cdot \sqrt{3} = \alpha_\tau \cdot \Delta\tau_{nom} \cdot \sqrt{3} \tag{7}$$

In Tab. 4 the outcome of an extensive experimental analysis of different chord-web junctions under pure bending or axial loading accounting for the mean stress influence is summarized [9]. The test results for weld toe failure and weld root failure fall into the same scatter band in this analysis. Unfortunately, it is unclear what failure hypothesis is used in [9] whether maximum principal stress or equivalent stress of DEH. Nevertheless, the corresponding fatigue strengths with 50 % probability of survival are computed in Tab. 4.

Since the mean stress influence in Tab. 4 is quite pronounced, the estimated size effect factor f_s is computed for $R = -1$ expecting no significant sensitivity of f_s on changes of the stress ratio R: $f_s = 486 / 484 \approx 1.0$. For comparison the tube-to-plate junctions in [11] have a comparable loading and a size factor $f_s = 1.39$.

Finally, the effective equivalent stress range $\Delta\sigma_{eq}(\delta = 0)$ at the upper weld toe can be computed to 823 N/mm² for weld 'A' and 700 N/mm² for weld 'B' using Eq. 5.

Table 3. Fatigue strength (N/mm²) at $N = 2 \cdot 10^6$ under shear loading, fillet welds, automatic welding, $R = -1$ [8]

Probability of survival	$\Delta\tau_{nom}$ [8]	Calculated $\Delta\tau_{notch}$	Calculated $\Delta\sigma_{eq,\,DEH}$
99.9 %	80	160	277
50 %	140	280	**484**

Table 4. Scatter band of fatigue strength under pure axial load or bending [3, 8]

Stress ratio	$R = -1$	$R = 0$	$R = +0{,}4$
scatter band parameter	1,44	1,42	1,55
average standard deviation	0,0652	0,0652	0,0652
$\Delta\sigma_{eq,97.7\%}$ (from [9])	360	260	210
$\Delta\sigma_{eq,50\%}$ (calculated)	**486**	351	284

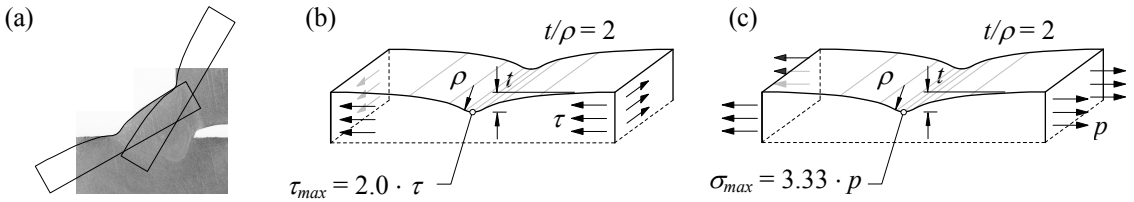

Figure 5. Section of crane rail weld (a), stress concentration of moderately curved notches under pure shear [7] p. 32 (b), under pure tension [7] p. 141 (c)

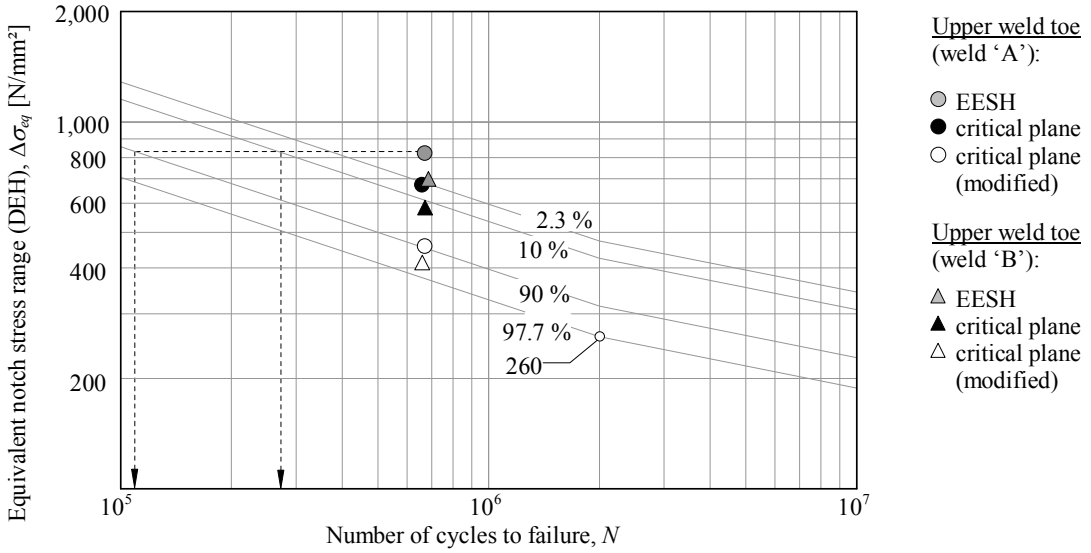

Figure 6. Scatter band of test results from [9] for $R = 0$, compare also Tab. 4.

CONCLUSIONS

Crane runways are subjected to a complex multiaxial state of stress due to geometric and metallurgic notch effects and the introduction of concentrated loads. The amplitudes of the stress components do not occur simultaneously resulting in an alternating direction of the shear stress that has been recognised to control the crack initiation. For two girder tests with in-phase interaction of the global bending σ_x and the local wheel pressure $\sigma_{z,local}$ the corresponding equivalent notch stress ranges according to DEH were computed applying two different local approaches. In Fig. 6 the computed stress ranges are plotted against the number of cycles to failure recorded in the tests. The findings are:

(i) Obviously, the critical plane approach according to *Findley* gives the best results falling between the lower and upper bound of the scatter band from literature.

(ii) The EESH results suggest that the crack initiation occurred earlier, Fig. 6. As the secondary cracks grew under compression (crack closing) they were very hard to detect. That is why an earlier crack initiation as recorded might be possible. On the other hand the lack of fatigue strength values under pure axial loading and pure shear for the

considered constructional detail have not allowed a reliable application of the EESH, yet. As the existing fatigue strengths for shear loading were primarily determined under torsion leading to crack opening modus III (Figs 7a and b) their usage for shear loadings that do not arise from torsion might be questionable. It is known that combined stresses solely induced by bending lead to crack opening modus I, Fig. 7c.

(iii) Further testing especially for out-of phase loading is necessary. In this case the secondary crack growth might be accelerated due to an interaction with the local shear stress $\tau_{xz,local}$ caused by the load application [6]. From that reason tests of crane runway girders under moving (reciprocating) single loads are planned for the near future.

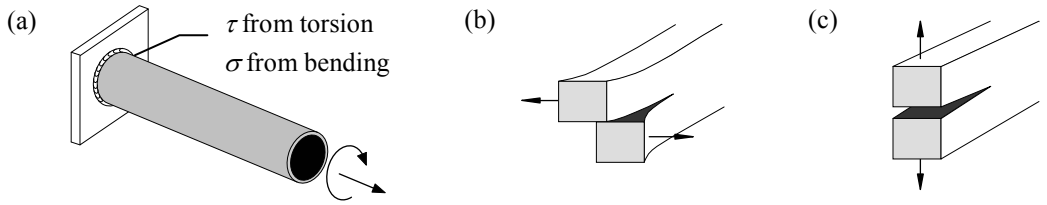

Figure 7. Typical test setup with combined direct stress due to bending and shear stress due to torsion (a), crack opening modus III (b) and modus I (c)

REFERENCES

[1] Euler M., Kuhlmann U. (2009). Crane runways – fatigue evaluation of crane rail welds using local concepts. In: Fatigue Design 2009, Senlis, Workshop W1, p. 1-10.

[2] Findley W. N. (1959). A theory for the effect of mean stress on fatigue of metals under combined torsion and axial load or bending. Transaction of the ASME. Journal of Engineering for Industry 81, p. 301-306.

[3] Köttgen V. B., Olivier R., Seeger T. (1991). Schwingfestigkeitsanalyse für Schweißverbindungen auf der Grundlage örtlicher Beanspruchungen. In: Berechnung, Gestaltung und Fertigung von Schweißkonstruktionen im Zeitalter der Expertensysteme Expert `91. DVS-Sondertagung, Essen, 20./21.02.1991. DVS report 133, p. 75-83.

[4] Kuhlmann U., Euler M. (2007). Kranbahnträger – Wirtschaftliche Bemessung und Konstruktion robuster Radlasteinleitungen. Research Report 5/2007 des Deutschen Ausschusses für Stahlbau (DASt), Stahlbau Verlags- und Service GmbH, Düsseldorf.

[5] Kuhlmann U., Euler, M. (2007). Multiaxial fatigue behaviour of hot-rolled crane runway beams with welded block rail. In: Fatigue Design 2007, Senlis, Workshop W1.3, p. 1-8.

[6] Maddox S. J., Razmjoo G. R. (2001). Interim fatigue design recommendations for fillet welded joints under complex loading. Fatigue and Fracture of Engineering Materials and Structures 24, p. 329-337.

[7] Neuber, H. (1985). Kerbspannungslehre. 3. Auflage, Springer-Verlag Berlin, Heidelberg.

[8] Seeger T., Olivier R. (1987). Ertragbare und zulässige Schubspannungen schwingbeanspruchter Schweißverbindungen. Stahlbau 56, No. 8, p. 231-238.

[9] Seeger T. (1996). Grundlagen für Betriebsfestigkeitsnachweise. In: Stahlbau-Handbuch, Teil 1B. Stahlbau-Verlagsges. mbH Köln.

[10] Sonsino C. M. (2009). Multiaxial fatigue assessment of welded joints – recommendations for design codes. Int. J. Fatigue 31, p. 173-187.

[11] Sonsino C. M. (1997). Schwingfestigkeit von geschweißten Komponenten unter komplexen elasto-plastischen, mehrachsigen Verformungen. Abschlussbericht, Europäische Kommission, Generaldirektion Wissenschaft, Forschung und Entwicklung, Schriftenreihe Technische Forschung Stahl, Luxembourg.

[12] Sonsino C. M. (2008). Suggested allowable equivalent stresses for fatigue design of welded joints according to the notch stress concept with the reference radii r_{ref} = 1.00 and 0.05 mm. International Insitute of Welding. Document XIII-2216-08/XV-1285-08.